



# Plasma-based dry reforming of methane in a dielectric barrier discharge reactor: Importance of uniform (sub)micron packings/catalysts to enhance the performance

Jinxin Wang<sup>a,b,1</sup>, Kaimin Zhang<sup>b,1</sup>, Myrjam Mertens<sup>c</sup>, Annemie Bogaerts<sup>a,\*</sup>, Vera Meynen<sup>b,c,\*\*</sup>

<sup>a</sup> Plasma Lab for Applications in Sustainability and Medicine - ANTwerp, Department of Chemistry, University of Antwerp, Universiteitsplein 1, Wilrijk, 2610 Antwerp, Belgium

<sup>b</sup> Laboratory of Adsorption and Catalysis, Department of Chemistry, University of Antwerp, Universiteitsplein 1, Wilrijk, 2610 Antwerp, Belgium

<sup>c</sup> Flemish Institute for technological research, VITO NV, Boeretang 200, 2400 Mol, Belgium

## ARTICLE INFO

### Keywords:

Dry reforming  
Plasma catalysis  
Uniform (sub)micron packing/catalysts  
Particle size effect  
Dielectric barrier discharge reactor

## ABSTRACT

This study presents new insights on the effect of (sub)micrometer particle sized materials in plasma-based CO<sub>2</sub>-CH<sub>4</sub> reforming by investigating the performance of SiO<sub>2</sub> spheres (with/without supported metal) of varying particle sizes. (Sub)micron particles synthesized through the Stöber method were used instead of (sub)millimeter particles employed in previous studies. Increasing particle size (from 120 nm to 2390 nm) was found to first increase and then decrease conversion and energy yield, with optimal performance achieved using 740 nm 5 wt% Ni loaded SiO<sub>2</sub>, which improved CO<sub>2</sub> and CH<sub>4</sub> conversion, and energy yield to 44%, 55%, and 0.271 mmol/kJ, respectively, compared to 20%, 27%, and 0.116 mmol/kJ in an empty reactor at the same flow rate. This is the first to achieve significant performance improvement in a fully packed reactor, highlighting the importance of selecting a suitable particle size. The findings can offer guidance towards rational design of catalysts for plasma-based reactions.

## 1. Introduction

The emission of greenhouse gases and the resulting climate change is a major issue for mankind. A lot of technologies are being studied for the conversion of greenhouse gases and the utilization of renewable resources, such as CO<sub>2</sub> hydrogenation and biomass conversion [1,2]. Among them, CO<sub>2</sub> reforming of methane (dry reforming) is an attractive technology since it simultaneously utilizes two greenhouse gases (CH<sub>4</sub> and CO<sub>2</sub>), which can come from sustainable resources such as biogas, to produce chemical products and clean fuels [3–8].

However, a large amount of energy is needed to activate the CH<sub>4</sub> and CO<sub>2</sub> because of their high stability. For example, classical thermocatalytic reactions always need a high temperature (> 800 °C), leading to problems like energy losses and catalyst deactivation. Non-equilibrium plasma catalysis is considered to be promising to overcome these problems, since CH<sub>4</sub> and CO<sub>2</sub> can be activated at a relatively low

temperature (lower than 250 °C) [9–12]. The accelerated electrons with high energy in plasma are able to dissociate the stable CH<sub>4</sub> and CO<sub>2</sub> molecules, while the other species with larger mass keep the overall kinetic temperature at a lower level [13–15]. Among the various types of non-equilibrium plasma reactors, the dielectric barrier discharge (DBD) reactor is one of the easiest to be combined with catalysts or packing materials, as it has a simple structure and operates at close to ambient temperature and atmospheric pressure [16–19].

Nevertheless, low conversion and energy yield (i.e., the amount of CO<sub>2</sub> and CH<sub>4</sub> converted per unit energy input) in a DBD reactor are its main drawbacks [20–22]. Using alumina dielectric material, Khoja et al., demonstrated relatively good performance with an energy yield of 0.085 mmol/kJ [23]. Tu et al., reported an energy yield of 0.19 mmol/kJ by altering the catalyst packing method [22]. Although using a lower specific energy input (SEI) could provide a higher energy yield in some studies [22,24,25], the conversion of CH<sub>4</sub> and CO<sub>2</sub> was

\* Corresponding author.

\*\* Corresponding author at: Laboratory of Adsorption and Catalysis, Department of Chemistry, University of Antwerp, Universiteitsplein 1, Wilrijk, 2610 Antwerp, Belgium.

E-mail addresses: [annemie.bogaerts@uantwerpen.be](mailto:annemie.bogaerts@uantwerpen.be) (A. Bogaerts), [vera.meynen@uantwerpen.be](mailto:vera.meynen@uantwerpen.be) (V. Meynen).

<sup>1</sup> These authors contributed equally to this work.

concomitantly reduced. Moreover, the existing catalysts and packing materials for DBD reactors have limited benefit in performance. In the majority of dry reforming studies with undiluted feed gases and fully packed fixed bed packings or catalysts, the conversion of CH<sub>4</sub> and CO<sub>2</sub> was lower than in the empty reactor at the same flow rate [22,24,26,27]. Table 1 shows a comparison of the conversion of CO<sub>2</sub> and CH<sub>4</sub> in empty and fully packed reactors, obtained from literature, at the same gas flow rates. Although the conversions of CH<sub>4</sub> and CO<sub>2</sub> vary in different papers depending on the operating conditions, a common feature is that the performance of fully packed reactors with catalyst/packing was not improved, and even more often decreased, compared to empty reactors. The positive effects of packings/catalysts in literature could often not compensate for the negative effects on converted amounts resulting from their filling in the reactor, thereby hindering their potential for industrial applications. Some literature reported that catalysts or packings improved the dry reforming conversion compared to empty reactors [13,28], but since the processes were performed at a constant space time, the gas flow rate was reduced to exclude the volume reduction caused by the packings or catalysts, resulting in a significant increase in SEI. Hence, it was not clear whether the improvement in conversion came from the packing/catalyst or from the higher energy input [29].

A main challenge in the study of plasma catalysts in DBD reactors is that the effect of the catalyst is much more complex than in thermal reactors. It is not only the reaction between activated molecules and the active components of the catalyst, but it also includes the influence of the catalysts on the plasma discharge. Various properties of the catalyst, such as the dielectric properties, shape, size and structure, have an effect on the plasma filamentary discharge, which is the main discharge mode in the DBD reactor, consisting of a number of independent micro-discharge filaments [29,32,33]. Several studies have reported the effect of packing materials without active catalytic element on the plasma reaction, to investigate the effect of possible catalyst supports on the discharge and to distinguish the physical and chemical effects of the interaction between the plasma and the catalyst. In some studies, the catalytically inactive dielectric supports showed even a better performance in terms of conversion than the supports loaded with metal active components, due to the physical influence on the discharge [19,30]. Simulation studies found that one of the important physical effects of the catalyst was the polarization of the dielectric packing in the electric field of the DBD reactor, generating an enhanced electric field near the contact points of the packing [34]. It was also proven in experiments that this effect changes the discharges and enhances the conversion [35,36]. Furthermore, the packing partially changes the plasma discharge mode in DBD reactors from filamentary discharge to a surface discharge [37], which may also be beneficial for plasma-based dry reforming [20,38,39]. However, the packing also reduces the available discharge volume,

and consequently the possible trajectories of micro-discharges, which has a negative effect on the plasma reaction [40]. In addition, for the same gas flow rate, it also reduces the space time of the feed gas in the plasma discharge area, which is also unfavorable for the conversion of the reagents [35,41].

These effects are greatly affected by the particle size of the packing materials and the catalysts. One of the reasons for the limited performance of the packings/catalysts might be that their positive effects are less important than negative effects, due to an inappropriate or non-uniform particle size [28,35]. There have been some studies on the size of the packing materials in plasma reactions, but the particle sizes in these studies were all in the millimeter or submillimeter range, which is relatively large for the gap dimensions (also in the millimeter range) of a common DBD reactor [28,29,32,42]. Therefore, their positive effect on the discharge behavior, such as turning filamentary discharges into surface discharges, may be small, leading to the existing studies on the effect of particle size in plasma reaction (not only plasma-based dry reforming, but also similar plasma reactions such as CO<sub>2</sub> decomposition) did not achieve good performance. Smaller particle sizes down to micron or submicron sizes have not yet been studied because they are considered to have too small void space and they are expected to reduce the space time too much, leading to too much negative effects in plasma catalysis, or even the prevention of plasma propagation between the particles [35,43,44]. However, in experiments, submicron or micron particles cannot achieve the closest packing in the reactor when loaded by tapping, so the void spaces and space times might not be too low.

Therefore, in this work, in order to improve the conversion and energy yield of dry reforming in DBD reactors, and to better understand the interaction of catalyst particles with the plasma and the influence of catalyst size, we use uniform silica spheres of submicron and micron size, to study the effect of support particles with different particle sizes on the plasma-based dry reforming. Furthermore, we also explore the changes after depositing a certain amount of catalytically active metal component on the silica support. All experiments were performed at constant gas flow rate and supplied power, so the applied specific energy was constant. The performance comparisons between the empty reactor and a packed bed reactor include the negative effects of fully packing the reactor, such as the greatly reduced space time.

## 2. Materials and methods

### 2.1. Preparation of samples

#### 2.1.1. Preparation of silica spheres

Ammonia solution (25 wt%), tetraethyl orthosilicate (TEOS), and ethanol were purchased from Sigma-Aldrich. Silica spheres with average

**Table 1**

Comparison of conversion of CO<sub>2</sub> and CH<sub>4</sub> in empty and fully packed DBD reactors at the same flow rate in literature of plasma-based dry reforming.

Performance of empty reactor		Performance of packed reactor			Reference
CO <sub>2</sub> conversion (%)	CH <sub>4</sub> conversion (%)	Packing/Catalyst	CO <sub>2</sub> conversion (%)	CH <sub>4</sub> conversion (%)	
22	33	γ-Al <sub>2</sub> O <sub>3</sub>	22	27	[30]
		Ag/γ-Al <sub>2</sub> O <sub>3</sub>	22	27	
		Pt/γ-Al <sub>2</sub> O <sub>3</sub>	22	33	
		Cu/γ-Al <sub>2</sub> O <sub>3</sub>	16	33	[19]
15	18	γ-Al <sub>2</sub> O <sub>3</sub>	12	15	
		Cu/γ-Al <sub>2</sub> O <sub>3</sub>	8	16	
		Au/γ-Al <sub>2</sub> O <sub>3</sub>	15	16	
		Pt/γ-Al <sub>2</sub> O <sub>3</sub>	13	17	
6	2	Ni-Mn/γ-Al <sub>2</sub> O <sub>3</sub>	2	4	[24]
20	37	ZrO <sub>2</sub>	12	27	
		SiO <sub>2</sub>	18	22	[28]
		α-Al <sub>2</sub> O <sub>3</sub>	22	33	
		BaTiO <sub>3</sub>	20	13	
8	23	Quartz Wool	3	24	[31]
		γ-Al <sub>2</sub> O <sub>3</sub>	3	8	
		Zeolite 3 A	2	3	

diameters of ~120 nm, ~460 nm, ~740 nm, and ~810 nm were synthesized by the traditional batched Stöber method [45], while silica spheres with average diameters of ~1.13  $\mu\text{m}$ , ~1.8  $\mu\text{m}$  and ~2.39  $\mu\text{m}$  were synthesized by a semi-batched modified Stöber method [46]. For the Stöber method, a certain amount of ammonia solution and water were dissolved in ethanol (see [45] for their ratio). The solution was agitated at 400 rpm and 20 °C, and 50 mL tetraethyl orthosilicate (TEOS) was added to it. Then, the solution was kept stirring at the same temperature for 24 h. Finally, it was centrifuged, and dried at 80 °C for 24 h to obtain silica spheres. In the semi-batched Stöber method proposed in the literature [46], 1.3 g of ~810 nm silica prepared by the batched Stöber method was dispersed in 22.6 mL ethanol solution with 0.7 mol/L  $\text{NH}_3$  and 8 mol/L  $\text{H}_2\text{O}$ , as a seed suspension. TEOS/ethanol solution in a volume ratio of 1:2 was slowly added into the stirring seed suspension at room temperature. After centrifugation and drying, silica spheres with diameters larger than 1  $\mu\text{m}$  were obtained. According to the average diameters of the silica spheres (in nm), the samples are denoted as Si-120, Si-460, Si-740, Si-810, Si-1130, Si-1800, and Si-2390, respectively.

### 2.1.2. Impregnation of metals on silica

Copper, iron, and nickel, as common dry reforming catalytically active metals, were supported on silica particles in this work. Copper nitrate trihydrate and ferric nitrate nonahydrate were purchased from Acros, and nickel nitrate hexahydrate was purchased from Sigma-Aldrich. The three metal nitrates were formulated into 100 mL separate precursor aqueous solutions. Then the silica spheres were dispersed in the precursor solutions with stirring for 5 h. The mass percentages of metal elements in solution relative to the  $\text{SiO}_2$  used for impregnation were 0.2%, 1% and 5%, respectively. After drying the full solution at 40 °C and calcination at 650 °C for 6 h, the metal oxide loading on the silica particles was obtained. The samples were reduced at 800 °C for 6 h in a tube furnace with 250 mL/min 2%  $\text{H}_2/\text{Ar}$ , before testing their catalytic performance in plasma dry reforming. They are denoted as  $\text{M}_x/\text{Si}-Y$ , where x is the mass percentage of metal to silica and Y is the diameter of the silica spheres in nm. For example, the silica spheres with a diameter of 740 nm supporting 1 wt% Ni are denoted as  $\text{Ni}_1/\text{Si}-740$ .

## 2.2. Catalyst and plasma characterization

Scanning electron microscopy (SEM) was performed by the FEI Quanta 250 field emission scanning electron microscope at an operating voltage of 20 kV. The diameter of more than 30 silica spheres in the electron microscope images were measured and averaged.

Nitrogen sorption was carried out on an automated gas sorption system (Quantachrome Quadrasorb SI). Before the measurements, the samples were degassed under high vacuum at 200 °C for 16 h. During the sorption measurements, the temperature was kept at -196 °C by liquid nitrogen. The surface area was determined by the multi-point Brunauer-Emmett-Teller (BET) method.

The metal-loaded samples were characterized by X-ray diffraction (XRD) on a Panalytical Empyrean PRO MPD diffractometer using  $\text{Co}$  radiation. The scanning speed for the continuous mode measurements was 0.07°/s. The XRD of all samples were measured after reduction at 800 °C. Some samples were re-calcined at 650 °C and then measured by XRD to compare their oxides, to prevent differences in the samples due to surface oxidation caused by storage in air.

Oxygen-temperature programmed oxidation ( $\text{O}_2$ -TPO) was performed for the metal-loaded samples on the ChemStar TPX Chemisorption Analyzer. The samples were degassed first at 200 °C for 1 h with 50 mL/min pure  $\text{He}$  flow. After cooling down to 50 °C, the  $\text{O}_2$ -TPO was carried out in 50 mL/min flow of 5%  $\text{O}_2/\text{He}$ , from 50 °C to 800 °C with 10 °C/min ramping rate.

Thermogravimetric analyses (TGA) were carried out on a Mettler Toledo TGA-DSC 3+, with a 80 mL/min flow of  $\text{O}_2$ . A heating rate of 10 °C/min from 30 °C to 800 °C was applied.

Electrical characterization of the plasma was monitored by part of the setup shown in Fig. 1. During the dry reforming test, the voltage was monitored by a high voltage probe (Tektronix, P6015A) and the current pulse was monitored by a Rogowski coil (Pearson 4100). The number of micro-discharges was obtained by counting the peaks per period in the current profile after excluding signal noise by applying a Savitzky-Golay filter of polynomial order 3 [29]. It should be noted that this is not the exact number of discharges in the reactor, but should be interpreted as apparent values. This is because the discharges might occur simultaneously, but only one current peak is shown in the current profiles, and some small discharges might be excluded as signal noise. However, multiple collections of current data and an average of the number of current peaks can be used to compare and study the effects of different samples on the discharge. A capacitor (10 nF) was connected in parallel with a low voltage probe (Picotech, TA150) and in series with the reactor to measure the dissipated charge in the plasma. The displaced charge of the discharge is the detected charge difference before and after discharge. An oscilloscope (Picotech, Picoscope 6402D) was used to collect all the signals and to show them on a PC. A Q-U graph, also known as a Lissajous figure, was plotted with the applied voltage (U) and dissipated charge (Q) as the horizontal and vertical axes, respectively. The power of the discharge generated in the DBD reactor, i.e. plasma power (P), can be determined from the area of Lissajous figures:

$$P = \frac{1}{T} \oint U(Q)dQ \quad (1)$$

The power of the power supply ( $P_s$ , supplied power) can be calculated from the applied voltage ( $U(t)$ ) and the current in the circuit ( $I(t)$ ):

$$P_s = \frac{1}{nT} \int_0^{nT} U(t)I(t)dt \quad (2)$$

The difference between the supplied power and the plasma power is the reactive power, that is the power that does not produce a discharge.

The counting and calculation of all electrical characteristics was completed by a MATLAB script [29].

## 2.3. Plasma dry reforming tests

A fixed bed DBD plasma reactor (illustrated in Fig. 1) was applied to test the performance of the samples for plasma-based dry reforming. A grounded stainless steel rod with a diameter of 13 mm was used as the inner electrode. An alumina tube with an outer diameter of 21.8 mm and an inner diameter of 17.41 mm was coaxially placed around the stainless steel inner electrode as a dielectric barrier, so the spacing between the inner electrode and dielectric barrier, which is the discharge gap, was about 2.2 mm. A stainless steel mesh was tightly wound around the alumina tube as an outer electrode and connected to a high voltage, supplied by a function generator (Tektronix, AFG 2021) and a high voltage amplifier (TREK, model 20/20 C-HS). The length of the outer electrode was 50 mm. The function generator provided an input signal with a frequency of 3 kHz, which was amplified by the amplifier. The electrical signals were collected by the oscilloscope and displayed on the PC to calculate the power in real time. The amplitude of the input signal from the amplifier was adjusted according to the calculation to keep the power of the power supply constant at 50 W. 6 g of silica spheres were filled in the entire plasma discharge space, and 2 g of glass wool was blocked at both sides to fix the spheres. The tapped volume of 6 g of silica spheres was larger than the volume of the discharge space (5.27 mL) for all particle sizes, to avoid the possible effect of glass wool on both sides on the discharge. Moreover, since the packing volume of the 6 g sample in the reactor is unknown, in order to calculate the packing density and space time, the samples were repacked in a volume equal to the discharge space (5.27 mL) of the reactor to measure the weight of the particles in the discharge space.

The silica spheres without supporting metal were tested directly in the DBD reactor. For the evaluation of silica with supporting metal, the

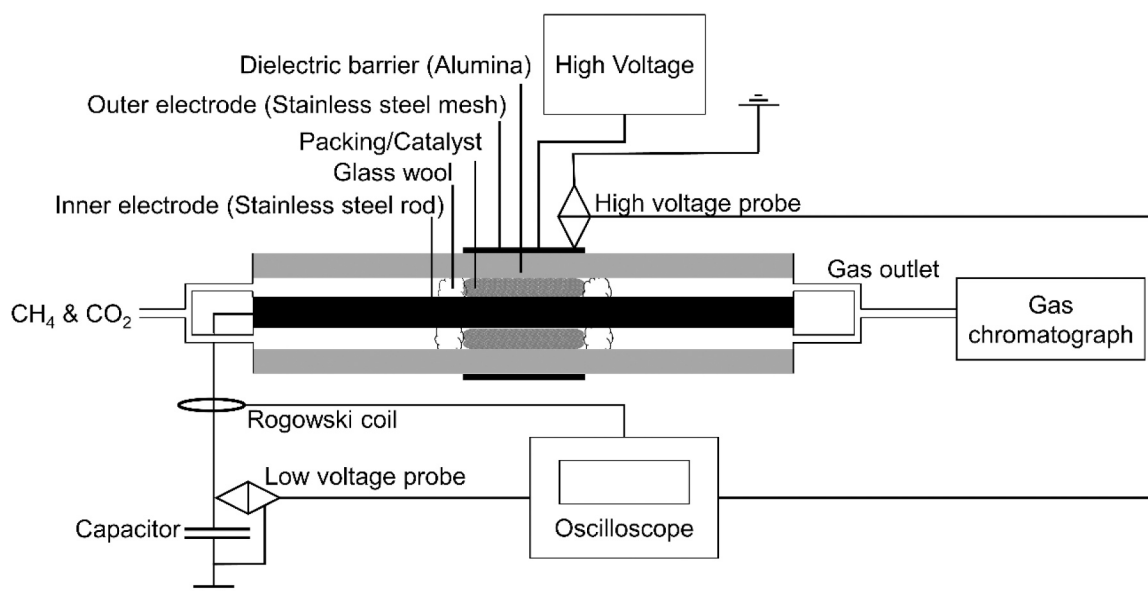


Fig. 1. DBD plasma set-up of the dry reforming tests.

samples were first reduced in a tube furnace (Carbolite Gero TF1 12/60/300) with 200 mL/min of 2% H<sub>2</sub>/Ar gas flow rate at 800 °C for 6 h before being packed into the reactor. The feed gas entering the reactor consisted of 10 mL/min of CH<sub>4</sub> and 10 mL/min of CO<sub>2</sub> controlled by mass flow controllers (Bronkhorst EL-FLOW Select). An online gas chromatograph (Trace GC 1310, Interscience) with a thermal conductivity detector (TCD) and a flame ionization detector (FID) was used to analyze the composition of the outlet gas. A digital pressure gauge was connected at the inlet of the GC to measure the pressure in the line. In all experiments, the measured pressure was ~1.05 atm regardless of whether the gas flowed through the bypass or the packed bed reactor. The composition of the feed gas was determined by the GC after the reactor was flushed for 30 min and before the plasma was turned on. The amounts of CO<sub>2</sub> and CH<sub>4</sub> in the feed gas were denoted as CO<sub>2,in</sub> and CH<sub>4,in</sub>, respectively. The power was then turned on to generate plasma and maintained at 50 W for 30 min to allow plasma stabilization. After that, the outlet gases were analyzed and marked with “out”, i.e., CO<sub>2,out</sub>, CH<sub>4,out</sub>, H<sub>2,out</sub>, CO<sub>out</sub> and C<sub>x</sub>H<sub>y</sub>O<sub>z,out</sub>. The conversion of CO<sub>2</sub> and CH<sub>4</sub> were defined as Eq. (1) and Eq. (2).

$$X_{CO_2}(\%) = \frac{CO_{2,in} - CO_{2,out}}{CO_{2,in}} \cdot 100\% \quad (3)$$

$$X_{CH_4}(\%) = \frac{CH_{4,in} - CH_{4,out}}{CH_{4,in}} \cdot 100\% \quad (4)$$

The (H-based) selectivity to H<sub>2</sub>, and the C-based selectivity to CO and of the other products were calculated by Eq. (3) to Eq. (5).

$$S_{H_2}(\%) = \frac{H_{2,out}}{2 \times (CH_{4,in} - CH_{4,out})} \cdot 100\% \quad (5)$$

$$S_{CO}(\%) = \frac{CO_{out}}{(CH_{4,in} - CH_{4,out}) + (CO_{2,in} - CO_{2,out})} \cdot 100\% \quad (6)$$

$$S_{C_xH_yO_z}(\%) = \frac{x \times C_xH_yO_{z,out}}{(CH_{4,in} - CH_{4,out}) + (CO_{2,in} - CO_{2,out})} \cdot 100\% \quad (7)$$

The energy yield (EY) of dry reforming was defined as the amount of CO<sub>2</sub> and CH<sub>4</sub> that can be converted per kJ of energy input in the plasma, as shown in Eq. (6).

$$EY(mmole/kJ) = \frac{(V_{CO_2}X_{CO_2} + V_{CH_4}X_{CH_4})}{PV_m} \cdot \frac{1000}{60} \left( \frac{Wmin}{kJ} \right) \quad (8)$$

Where V<sub>CO<sub>2</sub></sub> and V<sub>CH<sub>4</sub></sub> are the volumetric flow rate of CO<sub>2</sub> and CH<sub>4</sub> in the feed gas (in mL/min), and X<sub>CO<sub>2</sub></sub> and X<sub>CH<sub>4</sub></sub> are the conversion of CO<sub>2</sub> and CH<sub>4</sub>, respectively. P is the plasma power (in W) and V<sub>m</sub> is the molar gas volume (24.4 mL/mmol). Finally, the 1000/60 (Wmin/kJ) stands for the conversion of Wmin to kJ, in order to obtain the same units as in the left-hand side. Dry reforming produces CO, H<sub>2</sub> and unknown amounts of various hydrocarbons from CO<sub>2</sub> and CH<sub>4</sub>, causing an unknown coefficient of expansion and pressure increase in the outlet gas. The GC however always samples at a constant ambient pressure, so the gas composition analyzed by the GC has systematic errors. Therefore, 10 mL/min of N<sub>2</sub> was added into the outlet gas (without passing through the reactor) as an internal standard to correct for this and exclude the errors [47]. The amount of the components (e.g., CO<sub>2,in</sub>, CH<sub>4,in</sub>, H<sub>2,out</sub>, CO<sub>out</sub>) in the Eqs. (3)–(8) is the amount corrected using N<sub>2</sub> internal standard by the method reported in reference [47], which are also shown in Supporting Information (SI) as Eq. (S1)–(S3).

### 3. Results and discussion

#### 3.1. Particle size effect of the dielectric packing on plasma-based dry reforming

The morphology and size of the silica particles were measured by SEM. As shown in Fig. 2, all silica samples were of similar spherical shape with uniform diameters. The diameters of all measurable spheres (more than 30) on each SEM image were measured to calculate the average particle size and to plot the particle size distribution. The mean particle sizes were 120 nm, 460 nm, 740 nm, 810 nm, 1130 nm, 1800 nm, and 2390 nm, respectively, and were used to name these samples. The particle size distribution shown in Fig. 2h confirms that all samples were relatively uniform in size. The uniform size and shape made these samples suitable for studying the effect of the particle size in plasma-based dry reforming.

Fig. 3 shows the reforming conversion and energy yield for plasma-based dry for the empty reactor and the packed bed reactor with different sizes of silica spheres, at a constant 20 mL/min feed gas flow rate (1:1 of CH<sub>4</sub> to CO<sub>2</sub>) and 50 W applied power. Higher or at least comparable conversions of CH<sub>4</sub> and CO<sub>2</sub> were obtained for almost all diameters of the silica spheres compared to the empty reactor. This illustrates that the positive effects of the submicron and micron silica packing on the conversion were sufficient to compensate or even



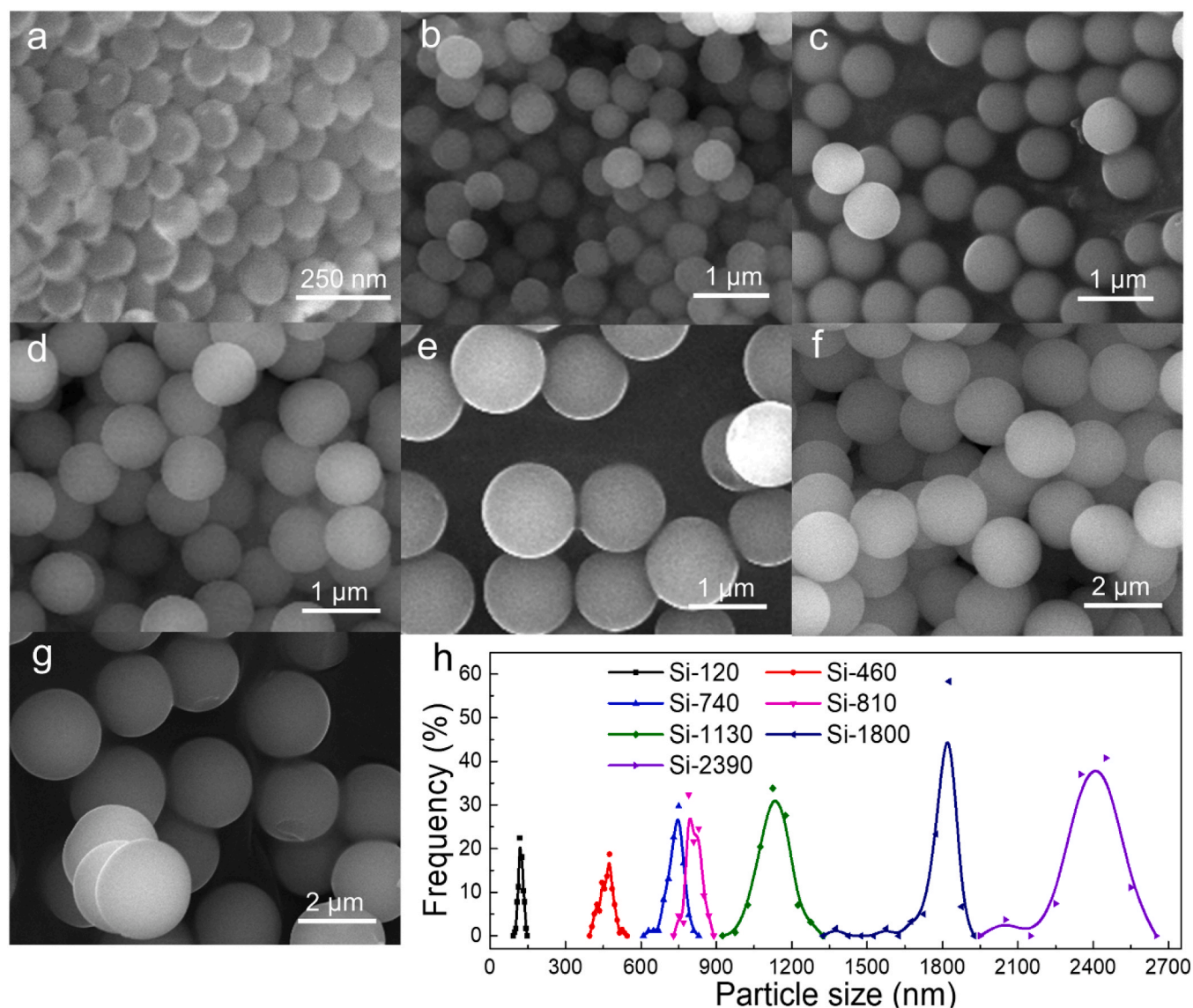
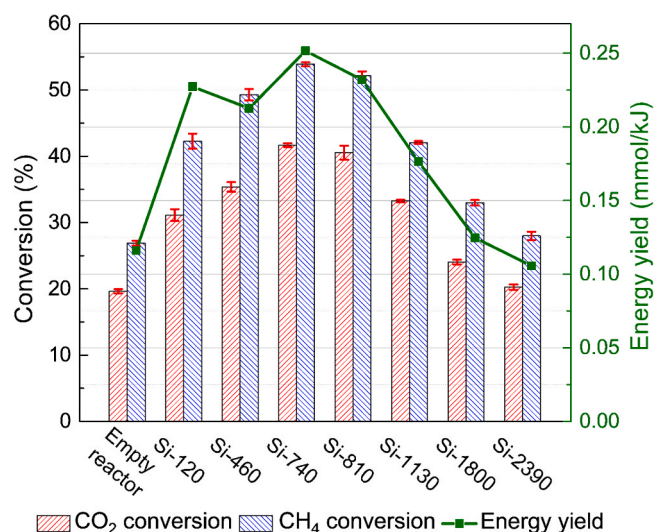


Fig. 2. SEM images of (a) Si-120, (b) Si-460, (c) Si-740, (d) Si-810, (e) Si-1130, (f) Si-1800 and (g) Si-2390. (h) Particle size distribution of all samples.

outweigh its negative effects (e.g., the reduction in space time) [22,29,32]. Moreover, the conversions of  $\text{CH}_4$  and  $\text{CO}_2$  first increase and then decrease with increasing diameter of the silica spheres. The silica spheres with a diameter of about 740 nm showed the highest conversion. More specifically, the  $\text{CO}_2$  and  $\text{CH}_4$  conversion raised from 20% and 27% in the empty reactor, to 42% and 54%, respectively. Since the experiments were performed at a constant supplied power and the same gas flow rate (not the same space time), the specific supplied energy in the empty reactor and for all packed reactors was constant. Nevertheless, the distribution, number and intensity of the discharges are different, resulting in different plasma powers at the same supplied power (see Table 2). The rest of the circuit was the same and each experiment was repeated three times, so we believe the different plasma power was due to the catalyst or packing and this is an important information for catalyst design. The portion of the supplied power that was not converted to discharge power was lost in the circuit as heat or returned to the source as reactive power. The energy yield followed a similar but not exactly correlated trend as the conversion due to the different plasma power. For example, since the plasma power generated in the reactor with Si-120 was significantly lower than that of the other samples, and possibly also due to its larger specific surface area (the effect of which will be explained below), the energy yield of Si-120 was

higher than that of Si-460, hence different from the conversion trend. The energy yield was improved from 0.116 mmol/kJ to a maximum of 0.252 mmol/kJ for the Si-740 packing. The effect of particle size on conversion included its effect on the discharge power generated in the reactor, while the energy yield showed the effect of particle size normalized by plasma power. With such a large effect of the submicron and micron range particle sizes on the conversion and energy yield, it is clear that non-uniform or inappropriate particle sizes in some plasma-catalytic studies might have been an important reason for the poor performance of catalysts in plasma-catalytic conversion [22,26,27].

Dielectric packing materials such as  $\text{SiO}_2$ , which have been commonly used as supports and were not considered catalytically active in dry reforming, improve the conversion of plasma-based dry reforming due to two possible effects. One is the enhanced electric field around the contact points between the packing particles, resulting from the polarization of the dielectric, which has a promoting effect on the conversion of  $\text{CH}_4$  and  $\text{CO}_2$  [34,35,48]. Another is the surface discharge on the packing particles. It has been reported that the plasma discharge mode in the DBD reactor was partially changed by the packing from a filamentary discharge, which is not energy efficient, to a surface discharge [22,31,37]. Both effects work better for smaller particles, which have



**Fig. 3.** Conversion of CH<sub>4</sub> and CO<sub>2</sub> (left y-axis) and energy yield (right y-axis) in plasma-based dry reforming, in the empty DBD reactor and the packed reactor with different particle sizes of SiO<sub>2</sub> at the same gas flow rate. The error bars were obtained from standard errors based on three repeat repacking experiments.

more contact points, smaller void spaces for filamentary discharge (determined by the particle size and packing density) and a larger external surface area in the same packing volume. The specific surface areas of the samples measured by N<sub>2</sub>-sorption are in Table 2. The nitrogen-sorption isotherms are shown in Supporting Information (SI), Fig. S1, which indicates that the SiO<sub>2</sub> samples are non-porous particles, except for the Si-120 which may have pores due to particle agglomeration.

However, as mentioned above, the tested conversion and particle size of the SiO<sub>2</sub> packing did not exhibit a simple linear relationship. This is because of the coinciding negative effects of the packing, which are also more pronounced in smaller particles. Possibly smaller void spaces between smaller particles limit more the trajectories of the discharge [40]. If the samples were packed with the closest packing in the reactor, the void spaces between Si-120 samples, with the smallest particle size, might be only tens of nm, and the plasma cannot even be generated and propagated in it because it is smaller than the Debye length [43,44]. Although the (sub)micron particles cannot achieve the closest packing in the reactor by tapping as mentioned above, and the fact that we have conversion and we see electrical signals characteristic for a discharge in the Si-120 packed reactor also proves that plasma can be generated, either in the void space or as surface discharges, the propagation of the plasma between the smaller particles is still expected to be more restricted due to their smaller void spaces. Moreover, the packing reduces the volume of the discharge space (from 5.27 cm<sup>3</sup> to ~ 3 cm<sup>3</sup>, calculated based on the occupied volume of the amount and density of

SiO<sub>2</sub>). Therefore, the gas passes through a smaller volume and the space time is reduced from ~15.8 s to ~ 4 s, which would lower the conversion [28,41]. At space times in the order of 20 s and less, small changes in space time are expected to decrease conversion substantially as it is further from partial equilibrium conditions [33]. The packing densities of SiO<sub>2</sub> particles, calculated from their weight in the discharge space and the volume of the discharge space in the reactor, are shown in Table 2. The smaller the SiO<sub>2</sub> particles, the more they are packed and the higher the packing density, resulting in a greater negative impact on the discharge. For the silica spheres with submicron and micron particle sizes used in this study, their positive effects on the discharge are dominant over the negative effects, so that higher energy yield and higher CH<sub>4</sub> and CO<sub>2</sub> conversion can be obtained at the same gas flow rate and power supply. The combined effect of the positive and negative effects of silica particles results in a first increase and then a decrease in conversion and energy yield with particle size.

Due to the limited measurement range of the PC connected oscilloscope system and the fluctuating discharge in the empty reactor, the connection between PC and oscilloscope was always broken. Hence, the displaced charge, and thus the Lissajous figures, of the empty reactor could not be obtained. The slopes of Lissajous figures obtained in the DBD reactor filled with SiO<sub>2</sub> particles with different sizes are shown in Fig. S2. More detailed data of the discharges, as obtained from the voltage, charge and current data are listed in Table 2. The plasma power was calculated by multiplying voltage and plasma current, and the average number of micro-discharges per period was the number of peaks in the normalized current profile after excluding signal noise [29]. The raw data of the Lissajous figures and voltage and current profiles for SiO<sub>2</sub> with different particle sizes in a period are shown in Fig. S3 and Fig. S4. As shown in Table 2, although the conversion in the empty reactor was lower than in the SiO<sub>2</sub> packed reactor, the root mean square current (RMS current) of the plasma was higher, and the applied peak-to-peak voltage (U<sub>pp</sub>) required to achieve the same supply power was lower. The plasma power and number of micro-discharges were also higher in the empty reactor compared to the packed reactor filled with particles with diameter smaller than Si-810. This indicates that the SiO<sub>2</sub> packing hindered the plasma discharge and maybe partially changed the filamentary discharge mode to surface discharge [22,31,36,37], and that the plasma discharged more often and was more powerful in the empty reactor.

The negative effects decreased with increasing particle size, which is also reflected in the electrical signal data in Table 2. Although there are exceptions, from Si-120 to Si-2390, the plasma power, plasma current, and number of micro-discharges all have a tendency to increase with increasing SiO<sub>2</sub> particle size, and the required peak-to-peak voltage decreases accordingly. This means that there is a higher energy input and a higher chance of individual discharges in the packed reactor with larger particle sizes [49]. It can be noticed from the Lissajous figures that the displaced charge (vertical distance between two vertices on the right side of the parallelogram) during the discharge also increased with the particle size. Dividing it by the number of micro-discharges yields the

**Table 2**

Specific surface area and packing density of the SiO<sub>2</sub> spheres with different diameters filled in the DBD reactor, as well as the electrical characterization data measured and calculated from the recorded signals of the oscilloscope of the dry reforming experiments.

	Power supplied (W)	Specific surface area (m <sup>2</sup> /g)	Packing density (g/cm <sup>3</sup> )	U <sub>pp</sub> (kV)	Plasma power (W)	RMS Current plasma (mA)	Number of micro-discharges (a.u./T)	Average filament charge (nC/disch.)
Empty reactor	50.4	/	/	18.8	27.4	24.5	75	/
Si-120	50.3	27	0.97	27.1	22.1	10.6	54	7.5
Si-460	50.5	6	0.96	23.2	27.2	12.6	70	8.4
Si-740	50.3	5	0.95	24.8	26.0	12.5	70	7.7
Si-810	50.7	4	0.95	24.3	27.3	10.8	76	7.0
Si-1130	50.1	4	0.91	21.0	29.2	16.2	72	10.5
Si-1800	50.3	3	0.85	20.3	31.3	14.4	80	10.4
Si-2390	49.7	3	0.84	20.0	31.2	14.3	74	11.0

average filament charge, which characterizes the strength of the discharge. The latter was also positively correlated with particle size. There was also a rough trend in the slopes on the left and right sides of the Lissajous figure, which increased slightly with particle size, indicating that the discharge fraction was larger in the reactor with large particles. These data verify that smaller particles are not conducive to discharge in DBD reactors, which is one of the reasons why the conversion and energy yield first increase with increasing particle size.

The selectivities of the main products formed in plasma-based dry reforming with the SiO<sub>2</sub> spheres of different particle sizes are shown in Fig. 4. It should be noted that the carbon and hydrogen mass balance calculated from the product selectivity does not reach 100% (shown in Fig. S5) because a few possible liquid products and carbon deposits attached to the catalyst and/or the reactor walls, as well as other gaseous products not calibrated in the gas chromatograph, could not be counted. As shown in Fig. 4a, for all SiO<sub>2</sub> particle sizes, the main product was syngas (CO and H<sub>2</sub>), and the CO selectivity was always higher than the H<sub>2</sub> selectivity (probably due to the formation of C<sub>2</sub>H<sub>6</sub> and C<sub>3</sub>H<sub>8</sub> or water, as shown in Fig. 4 and Fig. S5). Comparing the empty reactor and the packed reactor with silica particles of different sizes, the syngas selectivity appears to be related to the CH<sub>4</sub> and CO<sub>2</sub> conversions. Although there was not an accurate correspondence, there was a general trend that the lower the conversion of CH<sub>4</sub> and CO<sub>2</sub>, the greater the selectivity to CO and H<sub>2</sub>, i.e., the selectivity decreases first and then increases with increasing particle size. The selectivities of C<sub>2</sub>H<sub>6</sub>, CH<sub>3</sub>OH and C<sub>2</sub>H<sub>5</sub>OH (Ethanol, EtOH) also follow this trend (see Figs. 4b and 4c). As shown in Fig. 4b, the selectivity to C<sub>3</sub>H<sub>8</sub> and C<sub>2</sub>H<sub>4</sub> shows an increasing trend with increasing SiO<sub>2</sub> diameter, which might indicate that more micro-discharges or higher plasma power favor the formation of these two products. However, little C<sub>3</sub>H<sub>8</sub>, C<sub>2</sub>H<sub>4</sub> and C<sub>2</sub>H<sub>2</sub> (selectivity below 1%) were produced in the empty reactor despite it also having more micro-discharges and higher plasma power, probably due to the discharge mode in the empty reactor being different from the packed reactor. In addition, the voids between particles may also affect radical recombination and thus selectivity. Although the voids between particles (> tens of nanometers) are much larger than the diameter of the product molecule, we cannot exclude that enhanced collision with the surface might play a role.

### 3.2. Particle size effect of metal catalysts supports on plasma-based dry reforming

According to the above results, the SiO<sub>2</sub> spheres with a diameter of 740 nm show the highest conversion for both CO<sub>2</sub> and CH<sub>4</sub>, resulting from the combination of the positive and negative effects of the packing on the discharge. Supported metal catalysts are common traditional dry reforming catalysts. Therefore, Si-740 was used as a support to prepare metal loaded catalysts of Cu, Fe and Ni to test their performance in plasma-based dry reforming. The XRD patterns of catalysts loaded with 5% of the different metals are shown in Fig. S6. The dry reforming test conditions were the same as in Fig. 3. The obtained Lissajous figures and detailed electrical characteristics are shown Fig. S7, Fig. S8 and Table S1, respectively. Interestingly, as shown in Fig. 5, after loading with metal catalytic active components, the conversion of dry reforming was not improved in most samples, but decreased. Similar results have been reported in literature (e.g., [19,30]), which could be caused by the interaction between metal and plasma (i.e., changing surface discharges to local point-to-point discharge [50,51]), which may be detrimental to the dry reforming. Another possible explanation could be that, the metal catalyzed the reverse reaction of dry reforming. In the majority of cases of this study, the positive effects of catalytic activity cannot compensate for the negative effects of metal loading. Among these samples with different metals and different loadings, Ni<sub>5</sub>/Si-740 exhibits relatively better performance, and it was the only sample that improves the conversion of both CH<sub>4</sub> and CO<sub>2</sub> compared to unloaded Si-740 particles, under the here applied conditions. Due to the catalytic activity of the

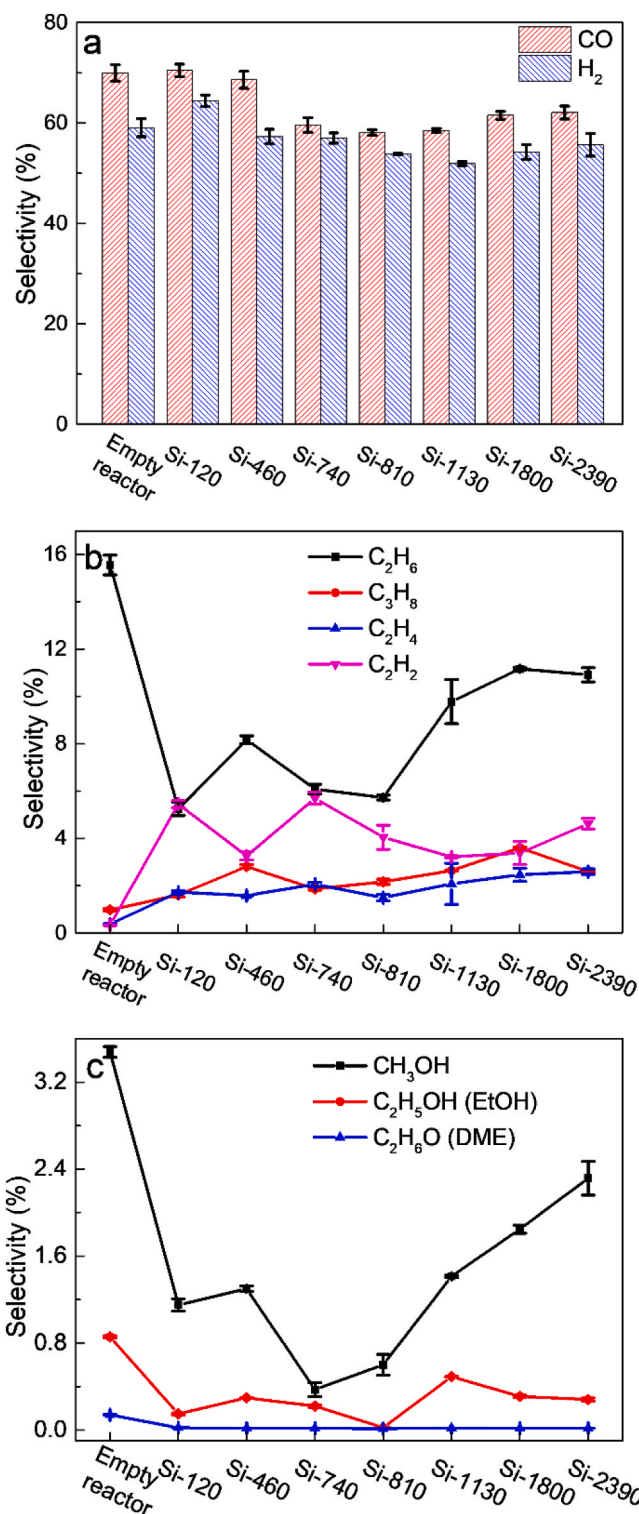
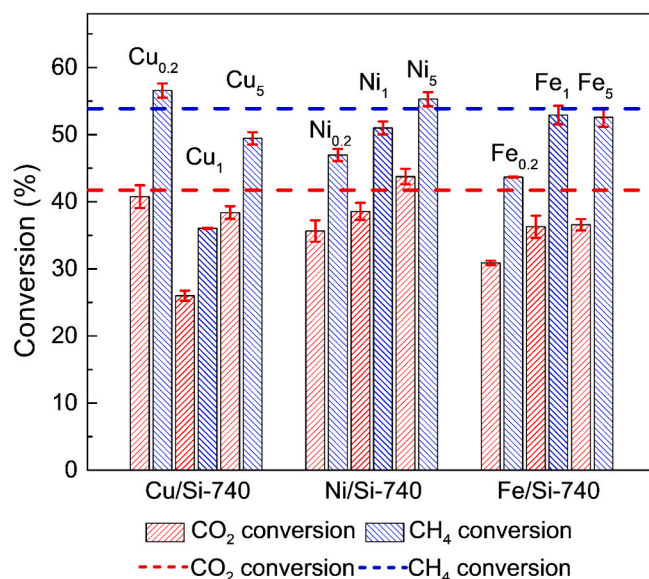


Fig. 4. Product selectivities in plasma-based dry reforming, in the empty reactor and the packed reactor with different particle sizes of SiO<sub>2</sub> spheres, for (a) CO and H<sub>2</sub>, (b) ethane, propane, ethylene, acetylene and (c) methanol, ethanol (EtOH) and dimethyl ether (DME). The error bars were obtained from standard errors based on three repeat repacking experiments.

metal and its interaction with the plasma, the role of the supported metal catalyst particles in the plasma-based dry reforming can be considered complex. Therefore, it is necessary to study whether the effect of the catalyst support particle size on the plasma-based dry reforming is still following the same trend as the pure silica packing.





**Fig. 5.** Conversion of CH<sub>4</sub> and CO<sub>2</sub> in plasma-based dry reforming of Si-740 without metal (benchmark – horizontal dashed line), and with different metals and loadings. The error bars were obtained from standard errors based on three repeat repacking experiments.

Silica spheres with all diameters were loaded with 5 wt% Ni and their catalytic performance for plasma-based dry reforming was tested. The test conditions were the same as in Fig. 3. The diameter of the particles with Ni (Fig. S9) was found not to have changed significantly compared to the pure SiO<sub>2</sub> particles. The XRD patterns and O<sub>2</sub>-TPO of Ni-loaded samples are shown in Fig. S10 and Fig. S11, respectively, and they do not show an obvious difference and trend for different support particle sizes. Hence, any differences observed in the plasma are most likely originating from differences in particles sizes. The variation of packing density (see Table 3 below) caused by the particle size is similar to that of the SiO<sub>2</sub> spheres without nickel loading. As shown in Fig. 6, similar to the unloaded silica particles, the conversion of CO<sub>2</sub> and CH<sub>4</sub> (including the effect of particle size on plasma power) and energy yield (showing the particle size effect normalized by plasma power) first increased and then decreased with increasing support particle size. The catalyst with support diameter of 740 nm still shows the best performance: it improves the CO<sub>2</sub> and CH<sub>4</sub> conversion from 20% and 27% in the empty reactor, to 44% and 55%, respectively. The energy yield reaches 0.271 mmol/kJ with the Ni<sub>5</sub>/Si-740 catalyst. Furthermore, not all sizes of supported Ni/SiO<sub>2</sub> catalysts perform better than the unloaded silica particles (see Fig. 3, also shown as dot lines in Fig. 6). The

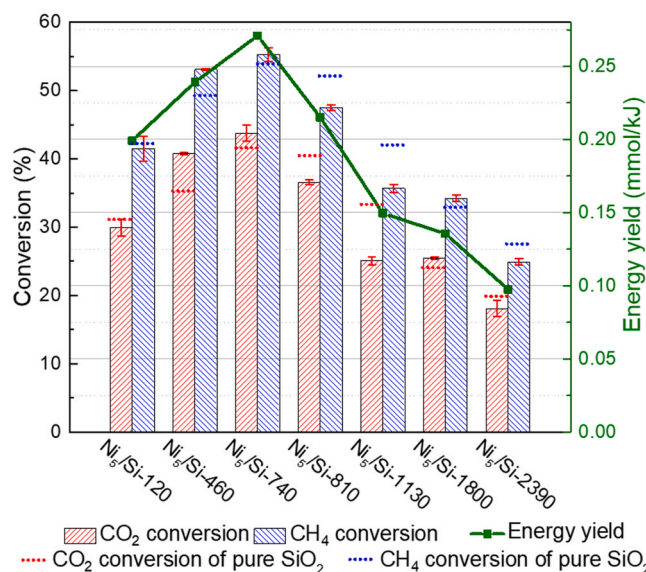


**Fig. 6.** Conversion of CH<sub>4</sub> and CO<sub>2</sub> (left y-axis) and energy yield (right y-axis) in plasma-based dry reforming with 5 wt% Ni loading on different particle sizes of SiO<sub>2</sub>. The error bars were obtained from standard errors based on three repeat repacking experiments.

conversion of dry reforming for Si-460, Si-740, and Si-1800 was improved after 5% Ni loading, but it decreased for Si-120, Si-810, Si-1130, and Si-2390 (relatively small changes for Si-120, Si-740 and Si-1800, less than 5%). The metal loading of differently sized particles not only changes the catalytic dry reforming activity of the silica particles, but also affects the plasma discharge [36,52]. The presence of the metal might enhance the electric field and electron density further in the proximity of the particle contact points, partially transforming the surface streamer discharges of the plasma on the dielectric into point-to-point local discharges [51,53,54]. Due to the size-dependent differences in properties, such as the number of contact points, void space and surface area, it could create a difference so that the effect of the interaction between metal and plasma was positive or negative on dry reforming, for particles with different diameters. Therefore, the change in conversion resulting from metal loading (i.e., the combined effect of metal catalytic activity and metal-plasma interaction) can be expected different for catalysts with different particle sizes. However, this change did not affect the trend of the material performance in function of particle diameters in our study. Which hints to a smaller, superimposed effect on plasma properties of the metal loaded packing compared to the impact of the size of SiO<sub>2</sub> support, while chemical

**Table 3**

Packing density of SiO<sub>2</sub> particles in the DBD reactor and electrical characterization data measured and calculated from the recorded signals of the oscilloscope of the dry reforming experiments with 5 wt% Ni loading on different particle sizes of SiO<sub>2</sub>.

	Power supplied (W)	Packing density (g/cm <sup>3</sup> )	U <sub>pp</sub> (kV)	Plasma power (W)	RMS Current plasma (mA)	Number of micro-discharges (a.u./T)	Average filament charge (nC/disch.)
Ni <sub>5</sub> /Si-120	50.6	0.93	25.2	24.5	11.9	75	8.0
Ni <sub>5</sub> /Si-460	50.5	0.94	24.1	26.8	12.3	72	8.2
Ni <sub>5</sub> /Si-740	50.0	0.92	25.4	25.0	11.4	79	6.4
Ni <sub>5</sub> /Si-810	50.5	0.93	23.1	26.7	14.0	79	9.2
Ni <sub>5</sub> /Si-1130	50.3	0.89	22.9	27.8	12.2	83	8.6
Ni <sub>5</sub> /Si-1800	50.3	0.85	21.5	30.1	12.8	91	8.4
Ni <sub>5</sub> /Si-2390	50.0	0.85	21.3	30.2	12.6	83	9.2



effects can still play an important role (see the changes in selectivity). The particle diameter of the packing/ support therefore is indeed an important factor in plasma-based dry reforming, even in supported metal catalysts.

The discharge data from the tests of the supported Ni catalysts in Fig. 6 are listed in Table 3 (the raw voltage and current profiles are shown in Fig. S12), and the slopes and raw data of Lissajous figures are shown in Fig. S13 and Fig. S14. It can be noticed from the table that the plasma current and average filament charge have no obvious trend with particle size, while other parameters, including plasma power, number of micro-discharges and peak-to-peak voltage, still follow a similar trend to those of the unloaded  $\text{SiO}_2$ , but with smaller differences. That is, the hindering effect of catalyst packing on the filamentary discharge decreases with increasing particle size, while less surface discharge might take place [22,31,36,37]. Compared with the pure  $\text{SiO}_2$ , the number of micro-discharges of the Ni-loaded  $\text{SiO}_2$  catalyst particles increased for all sizes, which could be attributed to the change of the plasma discharge induced by the metal, i.e., from surface discharge to point-to-point local discharge [50,51].

The product selectivities of  $\text{Ni}_5/\text{SiO}_2$  catalysts with different support particle sizes are shown in Fig. 7, and the carbon and hydrogen mass balances calculated from the product selectivity are shown in Fig. S15. Compared with unloaded pure  $\text{SiO}_2$ , the selectivity trend of  $\text{Ni}_5/\text{SiO}_2$  is not obvious. Although some products, such as  $\text{C}_2\text{H}_6$  and  $\text{CH}_3\text{OH}$ , still roughly follow a similar selectivity trend to the unloaded  $\text{SiO}_2$ , the differences between catalysts with different support diameters are not large (note the difference in Y-axis in Fig. 7 versus Fig. 4). This may be due to the reduced differences in electrical characteristic and the influence of metal catalytic activity on the reaction path [20,55–57]. The particles with different particle sizes support the same mass fraction of metal Ni, which might reduce the difference in product selectivity.

In addition, the stability of dry reforming performance of Si-740 and  $\text{Ni}_5/\text{Si-740}$  was studied. As shown in Fig. S16a, the conversion ( $\text{CO}_2$  and  $\text{CH}_4$ ) changes of both Si-740 and  $\text{Ni}_5/\text{Si-740}$  were less than 2% in 12 h DRM test. Fig. S16b shows the TGA-DTG results of Si-740 and  $\text{Ni}_5/\text{Si-740}$  before and after 12 h plasma dry reforming. As shown in Fig. S16b, used Si-740 lost less weight from 30 °C to 110 °C than fresh Si-740, indicating less water absorption on the surface of used Si-740. The weight change of Si-740 before and after DRM is almost the same after 110 °C. The  $\text{Ni}_5/\text{Si-740}$  before and after DRM also showed almost the same TGA curve. These indicate little carbon deposition on both Si-740 and  $\text{Ni}_5/\text{Si-740}$  during the 12 h DRM.

#### 4. Conclusion

In contrast to literature describing millimeter-sized packing materials, we synthesized uniform (sub)micron  $\text{SiO}_2$  spheres, ranging from 120 nm to 2390 nm in diameter, to be used as packing in DBD plasma-based dry reforming, and we deposited metals on these  $\text{SiO}_2$  particles to prepare supported catalysts. We found that due to their larger positive effect on the plasma discharge, packing the DBD reactor with uniform submicron and micron  $\text{SiO}_2$  spheres (including both  $\text{SiO}_2$  with or without metal loading) can achieve an increase in both conversion and energy yield of plasma-based dry reforming, from 20%  $\text{CO}_2$  conversion, 27%  $\text{CH}_4$  conversion and 0.116 mmol/kJ energy yield in the empty reactor, to a maximum of 44%  $\text{CO}_2$  conversion, 55%  $\text{CH}_4$  conversion and 0.271 mmol/kJ energy yield. The metal loading does not necessarily improve the dry reforming performance, and it may even reduce the  $\text{CH}_4$  and  $\text{CO}_2$  conversion due to the interactions between metal and plasma, even at small wt%.

We investigated the influence of packing/catalyst support particle size. We found that due to the balance between the promoting effects (e.g. enhancement of local electric field, change of discharge mode) and the hindering effects (e.g. restriction of the filament path and reduction of the space time) of the particle filling on the plasma discharge, the conversion of plasma-based dry reforming first increase and then decrease

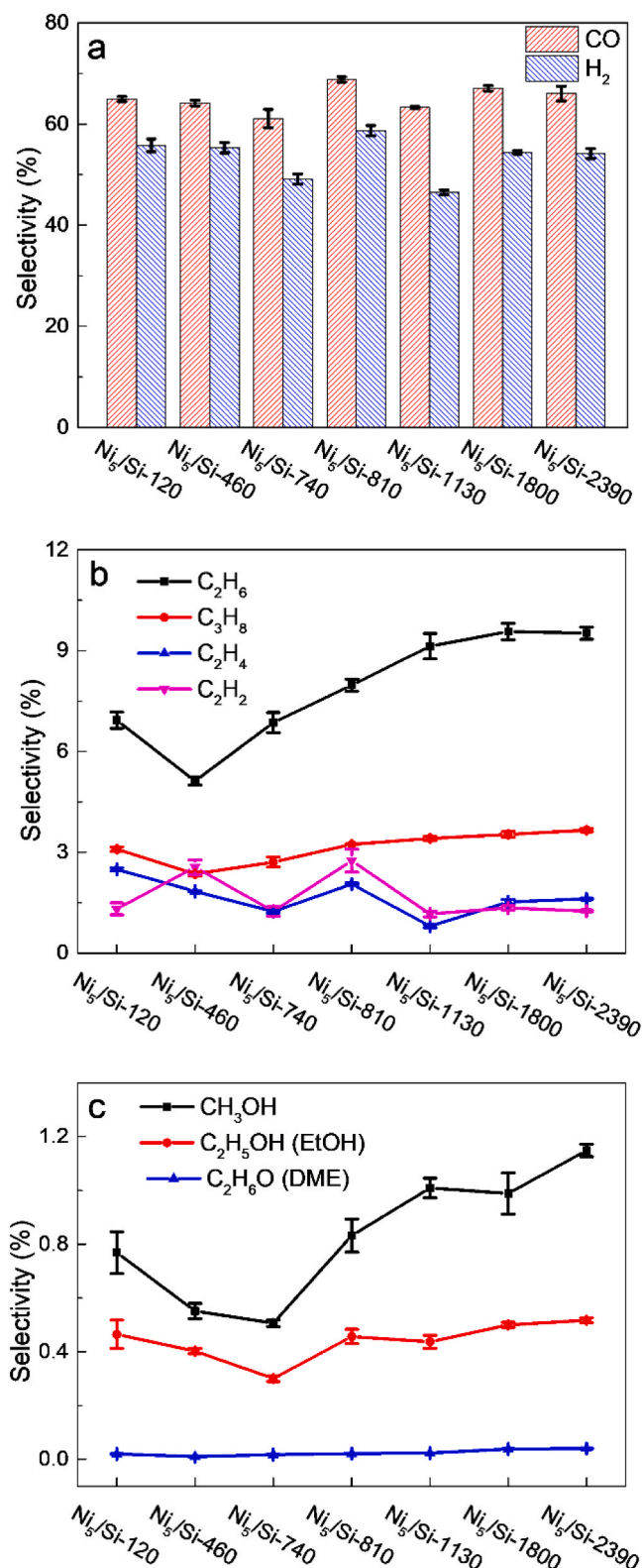


Fig. 7. Product selectivities in plasma-based dry reforming with 5 wt% Ni loading on different particle sizes of  $\text{SiO}_2$  spheres, for (a) CO and  $\text{H}_2$ , (b) ethane, propane, ethylene and acetylene, and (c) methanol, ethanol (EtOH) and dimethyl ether (DME). The error bars were obtained from standard errors based on three repeat repacking experiments.

with increasing particle size. There is an optimal particle size (possibly sub-micron), which may be different with different materials or reactor configurations, to maximize the conversion of CO<sub>2</sub> and CH<sub>4</sub>. In this study, both pure SiO<sub>2</sub> spheres and 5 wt% Ni-loaded SiO<sub>2</sub>, particles with a diameter of 740 nm exhibit the best performance. The particle size affects not only the conversion, but also the selectivity to various products. The effect on the selectivities may be attenuated by the metal loading as less influence on selectivity in function of particle size was observed.

In summary, submicron and micron silica spheres show good performance for plasma-based dry reforming either as dielectric packings or catalyst supports, and the particle size exhibits an important effect. It is important for plasma catalysis reactions in general to find a suitable particle size, as this can largely affect the performance. A suitable catalyst/packing particle size for plasma-based processes in DBD reactors might be in the sub-micron range, due to its large modification to filamentary discharge, rather than the millimeter-scale particles commonly used in the literature and in industrial applications. Moreover, plasma-catalyst interactions and discharge effects must be taken into account in the selection of active elements, as important negative effects might be present after active element loading.

### CRedit authorship contribution statement

**Jinxin Wang:** Conceptualization, Methodology, Investigation, Formal analysis, Validation, Visualization, Writing - original draft. **Kaimin Zhang:** Conceptualization, Methodology, Investigation, Formal analysis, Validation, Visualization, Writing - review & editing. **Myrjam Mertens:** Formal analysis, Visualization. **Annemie Bogaerts:** Supervision, Methodology, Resources, Writing - review & editing. **Vera Meynen:** Supervision, Methodology, Resources, Writing - review & editing.

### Declaration of Competing Interest

The authors declare that they have no known competing financial interests or personal relationships that could have appeared to influence the work reported in this paper.

### Data availability

Data will be made available on request.

### Acknowledgement

This work is supported by the China Scholarship Council (No. 201806060123); and the VLAIO Catalisti transition project CO2PERATE (HBC.2017.0692). K.Z acknowledges the EASiCHEM project funded by the Flemish Strategic Basic Research Program of the Catalisti cluster and Flanders Innovation & Entrepreneurship (HBC.2018.0484).

### Appendix A. Supplementary data

Supplementary data to this article can be found online at.

### Appendix A. Supporting information

Supplementary data associated with this article can be found in the online version at [doi:10.1016/j.apcatb.2023.122977](https://doi.org/10.1016/j.apcatb.2023.122977).

### References

- [1] S. Kattel, P. Liu, J.G. Chen, Tuning selectivity of CO<sub>2</sub> hydrogenation reactions at the metal/oxide interface, *J. Am. Chem. Soc.* 139 (2017) 9739–9754, <https://doi.org/10.1021/jacs.7b05362>.
- [2] M. Besson, P. Gallezot, C. Pinel, Conversion of biomass into chemicals over metal catalysts, *Chem. Rev.* 114 (2014) 1827–1870, <https://doi.org/10.1021/cr4002269>.
- [3] Y. Song, E. Ozdemir, S. Ramesh, A. Adishev, S. Subramanian, A. Harale, M. Albulai, A. Fadhel Bandar, A. Jamal, D. Moon, H. Choi Sun, T. Yavuz Cafer, Dry reforming of methane by stable Ni–Mo nanocatalysts on single-crystalline MgO, *Science* 367 (2020) 777–781, <https://doi.org/10.1126/science.aav2412>.
- [4] L. Zhou, J.M.P. Martinez, J. Finzel, C. Zhang, D.F. Swearer, S. Tian, H. Robotjazi, M. Lou, L. Dong, L. Henderson, P. Christopher, E.A. Carter, P. Nordlander, N. J. Halas, Light-driven methane dry reforming with single atomic site antenna-reactor plasmonic photocatalysts, *Nat. Energy* 5 (2020) 61–70, <https://doi.org/10.1038/s41560-019-0517-9>.
- [5] C. Palmer, D.C. Upham, S. Smart, M.J. Gordon, H. Metiu, E.W. McFarland, Dry reforming of methane catalysed by molten metal alloys, *Nat. Catal.* 3 (2020) 83–89, <https://doi.org/10.1038/s41929-019-0416-2>.
- [6] L.C. Buelens, V.V. Galvita, H. Poelman, C. Detavernier, G.B. Marin, Super-dry reforming of methane intensifies CO<sub>2</sub> utilization via Le Chatelier's principle, *Science* 354 (2016) 449.
- [7] J. Estephane, S. Aouad, S. Hany, B. El Khoury, C. Gennequin, H. El Zakhem, J. El Nakat, A. Aboukais, E. Abi Aad, CO<sub>2</sub> reforming of methane over Ni–Co/ZSM5 catalysts. Aging and carbon deposition study, *Int. J. Hydrog. Energy* 40 (2015) 9201–9208, <https://doi.org/10.1016/j.ijhydene.2015.05.147>.
- [8] H.U. Hambali, A.A. Jilil, A.A. Abdulrasheed, T.J. Siang, A.H.K. Owgi, F.F.A. Aziz, CO<sub>2</sub> reforming of methane over Ta-promoted Ni/ZSM-5 fibre-like catalyst: Insights on deactivation behavior and optimization using response surface methodology (RSM), *Chem. Eng. Sci.* 231 (2021), 116320, <https://doi.org/10.1016/j.ces.2020.116320>.
- [9] R. Snoeckx, A. Bogaerts, Plasma technology – a novel solution for CO<sub>2</sub> conversion? *Chem. Soc. Rev.* 46 (2017) 5805–5863, <https://doi.org/10.1039/C6CS00066E>.
- [10] A. Bogaerts, X. Tu, J.C. Whitehead, G. Centi, L. Lefteris, O. Guaitella, F. Azzolina-Jury, H.-H. Kim, A.B. Murphy, W.F. Schneider, T. Nozaki, J.C. Hicks, A. Rousseau, F. Thevenet, A. Khacef, M. Carreon, The 2020 plasma catalysis roadmap, *J. Phys. D: Appl. Phys.* 53 (2020), 443001, <https://doi.org/10.1088/1361-6463/ab9048>.
- [11] A. Bogaerts, E.C. Neyts, O. Guaitella, A.B. Murphy, Foundations of plasma catalysis for environmental applications, *Plasma Sources Sci. Technol.* 31 (2022), 053002, <https://doi.org/10.1088/1361-6595/ac5f8e>.
- [12] Y. Yi, X. Wang, A. Jafarzadeh, L. Wang, P. Liu, B. He, J. Yan, R. Zhang, H. Zhang, X. Liu, H. Guo, E.C. Neyts, A. Bogaerts, Plasma-catalytic ammonia reforming of methane over Cu-based catalysts for the production of HCN and H<sub>2</sub> at reduced temperature, *ACS Catal.* 11 (2021) 1765–1773, <https://doi.org/10.1021/acscatal.0c04940>.
- [13] Y. Uytendhousen, K.M. Bal, E.C. Neyts, V. Meynen, P. Cool, A. Bogaerts, On the kinetics and equilibria of plasma-based dry reforming of methane, *Chem. Eng. J.* 405 (2021), 126630, <https://doi.org/10.1016/j.cej.2020.126630>.
- [14] X. Tu, J.C. Whitehead, Plasma dry reforming of methane in an atmospheric pressure AC gliding arc discharge: Co-generation of syngas and carbon nanomaterials, *Int. J. Hydrog. Energy* 39 (2014) 9658–9669, <https://doi.org/10.1016/j.ijhydene.2014.04.073>.
- [15] Y. Yi, S. Li, Z. Cui, Y. Hao, Y. Zhang, L. Wang, P. Liu, X. Tu, X. Xu, H. Guo, A. Bogaerts, Selective oxidation of CH<sub>4</sub> to CH<sub>3</sub>OH through plasma catalysis: Insights from catalyst characterization and chemical kinetics modelling, *Appl. Catal. B Environ.* 296 (2021), 120384, <https://doi.org/10.1016/j.apcatb.2021.120384>.
- [16] Y. Uytendhousen, J. Hereijgers, T. Breugelmans, P. Cool, A. Bogaerts, How gas flow design can influence the performance of a DBD plasma reactor for dry reforming of methane, *Chem. Eng. J.* 405 (2021), 126618, <https://doi.org/10.1016/j.cej.2020.126618>.
- [17] F. Zhu, H. Zhang, X. Yan, J. Yan, M. Ni, X. Li, X. Tu, Plasma-catalytic reforming of CO<sub>2</sub>-rich biogas over Ni/γ-Al<sub>2</sub>O<sub>3</sub> catalysts in a rotating gliding arc reactor, *Fuel* 199 (2017) 430–437, <https://doi.org/10.1016/j.fuel.2017.02.082>.
- [18] M.-w. Li, G.-h. Xu, Y.-l. Tian, L. Chen, H.-f. Fu, Carbon dioxide reforming of methane using DC corona discharge plasma reaction, *J. Phys. Chem. A* 108 (2004) 1687–1693, <https://doi.org/10.1021/jp037008q>.
- [19] L. Wang, Y. Yi, C. Wu, H. Guo, X. Tu, One-step reforming of CO<sub>2</sub> and CH<sub>4</sub> into high-value liquid chemicals and fuels at room temperature by plasma-driven, *Catal., Angew. Chem. Int. Ed.* 56 (2017) 13679–13683, <https://doi.org/10.1002/anie.201707131>.
- [20] W.-C. Chung, M.-B. Chang, Review of catalysis and plasma performance on dry reforming of CH<sub>4</sub> and possible synergistic effects, *Renew. Sustain. Energy Rev.* 62 (2016) 13–31, <https://doi.org/10.1016/j.rser.2016.04.007>.
- [21] A.H. Khoja, M. Tahir, N.A.S. Amin, Recent developments in non-thermal catalytic DBD plasma reactor for dry reforming of methane, *Energy Convers. Manag.* 183 (2019) 529–560, <https://doi.org/10.1016/j.enconman.2018.12.112>.
- [22] X. Tu, J.C. Whitehead, Plasma-catalytic dry reforming of methane in an atmospheric dielectric barrier discharge: Understanding the synergistic effect at low temperature, *Appl. Catal. B Environ.* 125 (2012) 439–448, <https://doi.org/10.1016/j.apcatb.2012.06.006>.
- [23] A.H. Khoja, M. Tahir, N.A.S. Amin, Dry reforming of methane using different dielectric materials and DBD plasma reactor configurations, *Energy Convers. Manag.* 144 (2017) 262–274, <https://doi.org/10.1016/j.enconman.2017.04.057>.
- [24] D. Ray, P.M.K. Reddy, C. Subrahmanyam, Ni-Mn/γ-Al<sub>2</sub>O<sub>3</sub> assisted plasma dry reforming of methane, *Catal. Today* 309 (2018) 212–218, <https://doi.org/10.1016/j.cattod.2017.07.003>.
- [25] D. Ray, P. Manoj Kumar Reddy, S. Challapalli, Glass beads packed DBD-plasma assisted dry reforming of methane, *Top. Catal.* 60 (2017) 869–878, <https://doi.org/10.1007/s12444-017-0751-y>.
- [26] H.K. Song, J.-W. Choi, S.H. Yue, H. Lee, B.-K. Na, Synthesis gas production via dielectric barrier discharge over Ni/γ-Al<sub>2</sub>O<sub>3</sub> catalyst, *Catal. Today* 89 (2004) 27–33, <https://doi.org/10.1016/j.cattod.2003.11.009>.

- [27] J. Sentek, K. Krawczyk, M. Mlotek, M. Kalczyńska, T. Kroker, T. Kolb, A. Schenk, K.-H. Gericke, K. Schmidt-Szalowski, Plasma-catalytic methane conversion with carbon dioxide in dielectric barrier discharges, *Appl. Catal. B Environ.* 94 (2010) 19–26, <https://doi.org/10.1016/j.apcatb.2009.10.016>.
- [28] I. Michiels, Y. Uytendhouwen, A. Bogaerts, V. Meynen, Altering conversion and product selectivity of dry reforming of methane in a dielectric barrier discharge by changing the dielectric packing material, *Catalysts* 9 (2019), <https://doi.org/10.3390/catal9010051>.
- [29] Y. Uytendhouwen, S. Van Alphen, I. Michiels, V. Meynen, P. Cool, A. Bogaerts, A packed-bed DBD micro plasma reactor for CO<sub>2</sub> dissociation: Does size matter? *Chem. Eng. J.* 348 (2018) 557–568, <https://doi.org/10.1016/j.cej.2018.04.210>.
- [30] J.A. Andersen, J.M. Christensen, M. Østberg, A. Bogaerts, A.D. Jensen, Plasma-catalytic dry reforming of methane: Screening of catalytic materials in a coaxial packed-bed DBD reactor, *Chem. Eng. J.* 397 (2020), 125519, <https://doi.org/10.1016/j.cej.2020.125519>.
- [31] H.J. Gallon, X. Tu, J.C. Whitehead, Effects of reactor packing materials on H<sub>2</sub> production by CO<sub>2</sub> reforming of CH<sub>4</sub> in a dielectric barrier discharge, *Plasma Process. Polym.* 9 (2012) 90–97, <https://doi.org/10.1002/ppap.201100130>.
- [32] I. Michiels, Y. Uytendhouwen, J. Pype, B. Michiels, J. Mertens, F. Reniers, V. Meynen, A. Bogaerts, CO<sub>2</sub> dissociation in a packed bed DBD reactor: First steps towards a better understanding of plasma catalysis, *Chem. Eng. J.* 326 (2017) 477–488, <https://doi.org/10.1016/j.cej.2017.05.177>.
- [33] Y. Uytendhouwen, K.M. Bal, I. Michiels, E.C. Neyts, V. Meynen, P. Cool, A. Bogaerts, How process parameters and packing materials tune chemical equilibrium and kinetics in plasma-based CO<sub>2</sub> conversion, *Chem. Eng. J.* 372 (2019) 1253–1264, <https://doi.org/10.1016/j.cej.2019.05.008>.
- [34] K. Van Laer, A. Bogaerts, Fluid modelling of a packed bed dielectric barrier discharge plasma reactor, *Plasma Sources Sci. Technol.* 25 (2015), 015002, <https://doi.org/10.1088/0963-0252/25/1/015002>.
- [35] K. VanLaer, A. Bogaerts, Improving the conversion and energy efficiency of carbon dioxide splitting in a zirconia-packed dielectric barrier discharge reactor, *Energy Technol.* 3 (2015) 1038–1044, <https://doi.org/10.1002/ente.201500127>.
- [36] W. Wang, H.-H. Kim, K. Van Laer, A. Bogaerts, Streamer propagation in a packed bed plasma reactor for plasma catalysis applications, *Chem. Eng. J.* 334 (2018) 2467–2479, <https://doi.org/10.1016/j.cej.2017.11.139>.
- [37] H.J. Gallon, H. Kim, X. Tu, J.C. Whitehead, Microscope-ICCD Imaging of an Atmospheric Pressure CH<sub>4</sub> and CO<sub>2</sub> Dielectric Barrier Discharge, *IEEE Trans. Plasma Sci.* 39 (2011) 2176–2177, <https://doi.org/10.1109/TPS.2011.2157946>.
- [38] S. Zhang, Y. Gao, H. Sun, Z. Fan, T. Shao, Charge transfer in plasma assisted dry reforming of methane using a nanosecond pulsed packed-bed reactor discharge, *Plasma Sci. Technol.* 23 (2021), 064007, <https://doi.org/10.1088/2058-6272/abed30>.
- [39] D. Mei, X. Zhu, Y.-L. He, J.D. Yan, X. Tu, Plasma-assisted conversion of CO<sub>2</sub> in a dielectric barrier discharge reactor: understanding the effect of packing materials, *Plasma Sources Sci. Technol.* 24 (2014), 015011, <https://doi.org/10.1088/0963-0252/24/1/015011>.
- [40] X. Tu, H.J. Gallon, M.V. Twigg, P.A. Gorry, J.C. Whitehead, Dry reforming of methane over a Ni/Al<sub>2</sub>O<sub>3</sub> catalyst in a coaxial dielectric barrier discharge reactor, *J. Phys. D: Appl. Phys.* 44 (2011), 274007, <https://doi.org/10.1088/0022-3727/44/27/274007>.
- [41] A. Bogaerts, T. Kozák, K. van Laer, R. Snoeckx, Plasma-based conversion of CO<sub>2</sub>: current status and future challenges, *Faraday Discuss.* 183 (2015) 217–232, <https://doi.org/10.1039/C5FD00053J>.
- [42] M. El-Shafie, S. Kambara, Y. Hayakawa, Alumina particle size effect on H<sub>2</sub> production from ammonia decomposition by DBD plasma, *Energy Rep.* 6 (2020) 25–30, <https://doi.org/10.1016/j.egyr.2020.10.032>.
- [43] Q.-Z. Zhang, A. Bogaerts, Propagation of a plasma streamer in catalyst pores, *Plasma Sources Sci. Technol.* 27 (2018), 035009, <https://doi.org/10.1088/1361-6595/aab47a>.
- [44] Q.-Z. Zhang, A. Bogaerts, Plasma streamer propagation in structured catalysts, *Plasma Sources Sci. Technol.* 27 (2018), 105013, <https://doi.org/10.1088/1361-6595/aae430>.
- [45] W. Stöber, A. Fink, E. Bohn, Controlled growth of monodisperse silica spheres in the micron size range, *J. Colloid Interface Sci.* 26 (1968) 62–69, [https://doi.org/10.1016/0021-9797\(68\)90272-5](https://doi.org/10.1016/0021-9797(68)90272-5).
- [46] H. Giesche, Synthesis of monodispersed silica powders II. Controlled growth reaction and continuous production process, *J. Eur. Ceram. Soc.* 14 (1994) 205–214, [https://doi.org/10.1016/0955-2219\(94\)90088-4](https://doi.org/10.1016/0955-2219(94)90088-4).
- [47] N. Pinhão, A. Moura, J.B. Branco, J. Neves, Influence of gas expansion on process parameters in non-thermal plasma plug-flow reactors: A study applied to dry reforming of methane, *Int. J. Hydrog. Energy* 41 (2016) 9245–9255, <https://doi.org/10.1016/j.ijhydene.2016.04.148>.
- [48] H.L. Chen, H.M. Lee, S.H. Chen, M.B. Chang, Review of packed-bed plasma reactor for ozone generation and air pollution control, *Ind. Eng. Chem. Res.* 47 (2008) 2122–2130, <https://doi.org/10.1021/ie071411s>.
- [49] F.A. Herrera, G.H. Brown, P. Barboun, N. Turan, P. Mehta, W.F. Schneider, J. C. Hicks, D.B. Go, The impact of transition metal catalysts on macroscopic dielectric barrier discharge (DBD) characteristics in an ammonia synthesis plasma catalysis reactor, *J. Phys. D: Appl. Phys.* 52 (2019), 224002, <https://doi.org/10.1088/1361-6463/ab0c58>.
- [50] K. Van Laer, A. Bogaerts, How bead size and dielectric constant affect the plasma behaviour in a packed bed plasma reactor: a modelling study, *Plasma Sources Sci. Technol.* 26 (2017), 085007, <https://doi.org/10.1088/1361-6595/aa7c59>.
- [51] J. Kruselnicki, K.W. Engeling, J.E. Foster, M.J. Kushner, Interactions between atmospheric pressure plasmas and metallic catalyst particles in packed bed reactors, *J. Phys. D: Appl. Phys.* 54 (2020), 104001, <https://doi.org/10.1088/1361-6463/abcc92>.
- [52] A. Bogaerts, Q.-Z. Zhang, Y.-R. Zhang, K. Van Laer, W. Wang, Burning questions of plasma catalysis: Answers by modeling, *Catal. Today* 337 (2019) 3–14, <https://doi.org/10.1016/j.cattod.2019.04.077>.
- [53] W. Wang, T. Butterworth, A. Bogaerts, Plasma propagation in a single bead DBD reactor at different dielectric constants: insights from fluid modelling, *J. Phys. D: Appl. Phys.* 54 (2021), 214004, <https://doi.org/10.1088/1361-6463/abe8ff>.
- [54] T. Butterworth, R.W.K. Allen, Plasma-catalyst interaction studied in a single pellet DBD reactor: dielectric constant effect on plasma dynamics, *Plasma Sources Sci. Technol.* 26 (2017), 065008, <https://doi.org/10.1088/1361-6595/aa6c35>.
- [55] Z. Sheng, H.-H. Kim, S. Yao, T. Nozaki, Plasma-chemical promotion of catalysis for CH<sub>4</sub> dry reforming: unveiling plasma-enabled reaction mechanisms, *PCCP* 22 (2020) 19349–19358, <https://doi.org/10.1039/D0CP03127E>.
- [56] Z. Sheng, Y. Watanabe, H.-H. Kim, S. Yao, T. Nozaki, Plasma-enabled mode-selective activation of CH<sub>4</sub> for dry reforming: First touch on the kinetic analysis, *Chem. Eng. J.* 399 (2020), 125751, <https://doi.org/10.1016/j.cej.2020.125751>.
- [57] M. Shirazi, E.C. Neyts, A. Bogaerts, DFT study of Ni-catalyzed plasma dry reforming of methane, *Appl. Catal. B Environ.* 205 (2017) 605–614, <https://doi.org/10.1016/j.apcatb.2017.01.004>.